Journal of Alloys and Compounds 767 (2018) 1253–1263

Contents lists available at ScienceDirect

Journal of Alloys and Compounds

journal homepage: http://www.elsevier.com/locate/jalcom

Formation of bimetallic gold-silver nanoparticles in glass by UV laser irradiation

Maximilian Heinz [a], Vasiliy V. Srabionyan [b], Leon A. Avakyan [b], Aram L. Bugaev [c], Anna V. Skidanenko [b], Sviatoslav Yu Kaptelinin [b], Jürgen Ihlemann [d], Jörg Meinertz [d], Christian Patzig [e], Manfred Dubiel [a], Lusegen A. Bugaev [b, *]

[a] Institute of Physics, Martin Luther University Halle-Wittenberg, Von-Danckelmann-Platz 3, D-06120 Halle (Saale), Germany
[b] Department of Physics, Southern Federal University, Zorge Str. 5, RU-344090 Rostov-on-Don, Russia
[c] The Smart Materials Research Center, Southern Federal University, Sladkova 178/24, RU-344090 Rostov-on-Don, Russia
[d] Laser-Laboratorium Göttingen e.V., Hans-Adolf-Krebs-Weg 1, D-37077 Göttingen, Germany
[e] Fraunhofer Institute for Microstructure of Materials and Systems IMWS, Walter-Hülse-Str. 1, D-06120 Halle (Saale), Germany

ARTICLE INFO

Article history:
Received 5 May 2018
Received in revised form
1 July 2018
Accepted 15 July 2018
Available online 17 July 2018

Keywords:
AuAg nanoparticles
Surface plasmon resonance
UV laser processing
XAFS
Optical spectroscopy

ABSTRACT

Experimental technique for preparing of space arranged arrays of bimetallic AuAg nanoparticles in the near-surface region of glass, exhibiting surface plasmon resonance (SPR) characteristics varying in the wider ranges comparing to monometallic Au, Ag particles or corresponding thin films, is presented together with the structural characterization of the obtained particles. The suggested technique is based on the UV laser irradiation ($\lambda = 193$ nm) of the glass surface preliminary doped with silver ions and then sputter coated by a thin gold layer. Optical extinction spectra of the prepared AuAg/glass samples demonstrated strong dependence of SPR upon the number of laser pulses applied. The relationship "SPR characteristics – particles structure and composition – synthesis conditions" was studied using transmission electron microscopy (TEM), energy-dispersive X-ray spectroscopy (EDX), X-ray fluorescence (XRF) method and X-ray absorption fine structure (XAFS) spectroscopy. The latter provided the structural information on Au–Ag bonds, which directly evidenced on the formation of bimetallic AuAg nanoparticles in AuAg/glass samples. The XAFS derived values of structural parameters of Au–Au and Au–Ag bonds allowed to visualize the distribution of gold and silver over the volume of representative AuAg nanoparticle and to suggest the most plausible cluster models of the architecture of such particle for the prepared AuAg/glass samples. It was revealed that the core-shell architecture of Au@Ag particles (Au-core, Ag-shell) is the most plausible in AuAg/glass samples prepared by the low number of laser pulses, while the structure of disordered solid solution is suitable for AuAg particles in samples prepared by ~ 50 and more pulses. Calculations of contributions into experimental optical extinction spectra of AuAg/glass samples from particles with the revealed composition, size and architecture were performed to prove that the proposed structural models of nanoparticles are not in contradiction with the observed optical properties of the samples.

1. Introduction

Gold and silver nanoparticles find wide applications in photocatalysis [1,2] and electrocatalysis [3–5], as sensors in chemistry [6,7] and biology [8,9], in medicine [10,11], and in a variety of optical devices due to their linear and nonlinear optical properties, such as the surface plasmon resonance (SPR) [12–14], which enables to localize electromagnetic field on nano-scales. Shape and wavelength position (λ_{SPR}) of SPR depend on the size and shape of the nanoparticles, degree of their agglomeration [15,16], and hence can be tuned by choosing the synthesis conditions, which is especially important for the construction of information storage and processing devices [17], development of subwave optical devices, plasmon nano-antennas [18,19], nano-lasers, elements of optical circuits and photodetectors.

The properties and the efficiency of the materials based on gold and silver nanoparticles can be improved and enhanced by using bimetallic AuAg particles instead of the monometallic ones.

* Corresponding author.
E-mail address: bugaev@sfedu.ru (L.A. Bugaev).

https://doi.org/10.1016/j.jallcom.2018.07.183
0925-8388/

Calculations of optical extinction spectra for different hypothetical core-shell models of AuAg nanoparticles by generalized multiparticle Mie theory [20] revealed that due to the difference in light scattering and absorption by gold and silver atoms [16], the SPR parameters can be changed in wide ranges depending upon the structural parameters of core and shell so, that the shift of λ_{SPR} can be of ~ 3–4 times larger than in the corresponding monometallic particles or in thin films [21]. Various experimental techniques for production of bimetallic nanoparticles in different dielectric matrices or on different supports were suggested, including the simultaneous or sequential deposition of metals to form particles with a solid solution or core-shell structures [22–24]. However, to obtain submicron line patterns of spatially arranged arrays of plasmonic nanoparticles in the near-surface region of glass, it is preferable to use the approach which is based on the irradiation of the preliminary prepared glass by UV laser with energy below the ablation threshold, using corresponding laser masks or gratings [25,26]. By this approach, arrays of monometallic silver and gold nanoparticles in the near-surface region of silicate glass were obtained using ArF-excimer laser irradiation (193 nm) for i) the glass containing Ag^+ ions, preliminary incorporated due to $Ag^+ \leftrightarrow Na^+$ ion exchange to produce Ag particles [26] and ii) the glass sputter coated with a 70 nm gold layer to produce Au particles [27].

In this work, these two techniques are combined to produce the arrays of bimetallic AuAg nanoparticles in the near-surface glass region via laser irradiation of silver-doped silicate glass sputter coated with a thin gold layer. The used approach is promising since the gold particles formed in the near-surface glass region after the first few laser pulses [27] can be considered as the suitable substrates or nuclei for precipitation of the reduced silver atoms on them. The procedure for obtaining the bimetallic AuAg particles and adopted characterization techniques are described in Sec. 2. Transmission electron microscopy (TEM) images, evidencing the particle formation, together with the optical extinction spectra of samples obtained by different number of laser pulses are reported in Sec. 3.1, demonstrating the appearance and transformation of SPR with the increasing number of laser pulses. However, the suggested experimental technique can result in the formation of different types of particles: monometallic gold or silver and bimetallic AuAg nanoparticles with the structure ranging from disordered solid solutions to core-shell architectures. Under such a variety of possible structures, the formation of bimetallic AuAg particles is studied by energy-dispersive X-ray spectroscopy (EDX), X-ray fluorescence (XRF) and Ag *K*-edge X-ray absorption spectra. To obtain direct evidence of the formation of AuAg nanoparticles – the presence of significant amount of Au-Ag bonds in the sample, the structural characterization of Au-containing particles in AuAg/glass samples prepared at different number of laser pulses is performed by X-ray absorption near edge structure (XANES) and by X-ray absorption fine structure (EXAFS) in Au L_3-edge absorption spectra (Sec. 3.2). The EXAFS derived structural parameters are used to visualize the components (Au and Ag) distribution over the volume of representative AuAg nanoparticle and to reveal the most plausible cluster models of this particle's architecture for each AuAg/glass sample (Sec. 3.3). Calculations of contributions into experimental optical extinction spectra of AuAg/glass samples from particles with the revealed composition, size and architecture are performed (Sec. 3.4).

2. Experimental and theoretical methods

2.1. AuAg/glass samples preparation and experimental measurements

The detailed description of the experimental techniques and the study of the formation of silver and gold nanoparticles in the near-surface region of silicate glass by UV laser radiation (193 nm) was performed respectively in Refs. [26,27]. In this work, we have combined these techniques for the creation of bimetallic AuAg nanoparticles in soda-lime silicate float glass by laser irradiation. The commercial float glass with thickness of 1 mm had the following composition (the values are given in weight %): 72.3% SiO_2, 0.5% Al_2O_3, <0.02% Fe_2O_3, 13.3% Na_2O, 8.8% CaO, 0.4% K_2O, 4.3% MgO. In addition, one side of the glass contains 0.02 wt. % of SnO_2, this side will be further referred as tin-bath side. The opposite side (without tin) will be referred as air-side. At the first step, silver/sodium ion exchange procedure ($Ag^+ \leftrightarrow Na^+$) was applied to dope the glass slides by silver ions [26–29]. Then, tin-bath sides of the both silver-doped and pure glass samples were sputter coated with gold by means of K550 Sputter Coater system (manufactured by Quorum Technologies) using the plasma current of 20 mA and Ar pressure of 10^{-1} mbar. As we have demonstrated before, this procedure produces a 70 nm gold layer on the tin-bath glass surface [27]. As a final step, a 193 nm ArF-excimer laser irradiation (LPX 315 laser, manufactured by Lambda Physik) with 20 ns pulse duration was applied to the induce formation of silver and gold nanoparticles in the samples. For each sample, the different number of laser pulses was applied in the range from 0 to 1000, with pulse repetition rate of 1 Hz. In all cases, the tin-bath side of the glass was exposed to the laser pulses. The size of the laser spot on the sample surface was in the rage of 6×6 mm^2 to 10×10 mm^2. The average laser fluence was 140 mJ/cm^2. As the fluence of the first laser pulse was shown to affect significantly the nanoparticle formation process [27], the actual fluence of each laser pulse was measured simultaneously using a beam splitter, and the fluence of the first laser pulse was ensured to be equal to 140 mJ/cm^2 for each studied sample. As revealed by TEM and EXAFS studies (vide infra) this procedure leads to the formation of the Ag, Au and AuAg nanoparticles in the near-surface glass region. Non-implanted particles located on the surface were removed mechanically by cleaning with acetone.

Analytical (scanning) transmission electron microscopy ((S)TEM) measurements including EDX-analysis were performed using a FEI Titan3 80–300 electron microscope operated at an acceleration voltage of 200 kV. STEM images were obtained using a high-angle annular dark field detector (HAADF, Fischione Model 3000). EDX was performed using a Super-X EDX detector equipped with four SDD detectors (FEI Company). The STEM sample preparation was done by a purely mechanical wedge-polishing routine (polishing system MultiprepTM, Allied company), followed by a low-energy (2.5 keV) Ar^+ broad beam final milling step (precision ion polishing system PIPS, Gatan company) to achieve electron transparency and to remove any residues from the mechanical polishing. To provide electric conductivity during the STEM investigations the samples have been coated with a thin carbon layer.

Optical extinction spectra have been measured by Lambda 900 UV/Vis/NIR spectrometer (Perkin Elmer) in the wavelength range from 300 nm to 800 nm. To reduce the spot size to the laser irradiated areas a circular aperture with a diameter of 3 mm has been used.

Au L_3-edge X-ray absorption spectra were measured at the BM23 beamline (Proposal MA 3438) and **Ag *K*-edge X-ray absorption spectra** were measured at BM26A beamline (Proposal CH 5046) of the European Synchrotron Radiation Facility (ESRF, Grenoble, France). All spectra were measured at room temperature. Due to the low concentration of the nanoparticles and their location in the surface layer of the glass, the spectra were collected in fluorescence yield mode. The photon energy scanning steps were adjusted to $\delta E = 1.0$ eV and $\delta k = 0.05$ Å^{-1} in the XANES and EXAFS regions respectively, where E is the energy of the incident radiation

and k is the corresponding photoelectron wavenumber.

XRD patterns were collected by Bruker D2 PHASER diffractometer with Cu K_α source ($\lambda = 1.5418$ Å) in a similar way as was described in Ref. [27].

2.2. Theoretical approaches to X-ray absorption spectra analysis. Modeling of bimetallic nanoparticles and their optical extinction spectra

Structural characterization of nanoparticles in AuAg/glass samples was performed using XANES and EXAFS regions of Au L_3-edge absorption spectra and Ag K-edge EXAFS spectra.

Au L_3-edge XANES were analyzed via fitting of the experimental spectra by theoretical ones using multidimensional interpolation approach [30] of FitIt code [31]. The theoretical spectra for pure Au nanoparticles and single Au atom surrounded by Ag atoms were calculated in FEFF9 code [32,33]. The spectra corresponding to the intermediate Ag/Au stoichiometries (in the range from 0 to 1) were obtained by linear interpolation of the calculated ones. Based on the previous studies [26,27] and the comparative analysis of the Fourier-transforms $F(R)$ of EXAFS spectra of Au-foil and of the studied AuAg/glass samples in the extended range of interatomic distances (R) (vide infra), the *fcc*-like 135-atoms metal clusters with the lattice parameter of 4.09 Å were used for FEFF calculations. To enhance the effect of formation of mixed AuAg NPs on the shape of XANES spectra, the fitting was performed using difference XANES spectra [34,35], obtained by subtracting the experimental spectrum of pure Au nanoparticles and the calculated spectrum of pure Au from all experimental and theoretical spectra, respectively.

The processing of EXAFS in bimetallic nanoparticles requires a large number of structural and non-structural parameters which usually strongly correlate. To reduce the effect of these correlations on the obtained values of structural parameters, the experimental spectra were processed using the technique [29,36]. For the local structures of each type of the absorbing atoms in bimetallic nanoparticle, the used technique provides a high accuracy of structural parameters determination: for interatomic distances $\Delta(R) \sim 0.01$ Å and for partial coordination numbers up to $\delta(N) \sim 7\%$. In contrast to Au L_3-EXAFS spectra, which give the structural parameters of Au–Au and Au–Ag bonds, analysis of Ag K-edge EXAFS in AuAg/glass samples is extremely complicated since most of the silver atoms (more than 90%) in the form of ions are interacting with oxygen of the glass matrix and such a background of Ag–O bonds makes extremely complicated the processing of Ag K-edge EXAFS for determination of structural parameters of Ag–Ag and Ag–Au bonds in bimetallic nanoparticles with acceptable accuracy. However, one can estimate the percentage of silver atoms in nanoparticles by the fit of the dominating Ag–O contribution in the Fourier-transform (FT) function F(R) of Ag K-edge EXAFS in the laser irradiated AuAg/glass samples using the approach suggested in Ref. [29], which enables to reduce significantly the number of fit variables by employing oscillatory part $\chi^{\mathrm{Exper.}(N=0)}{}_{\mathrm{Ag}}(k)$ of experimental Ag K-edge EXAFS-spectrum of the non-irradiated (number of laser pulses $N = 0$) glass sample as the fixed function (experimental standard) in the fitting procedure based on the expression:

$$\chi^{(N)}_{Ag}(k) = C\cdot\chi^{Exper\cdot(N=0)}_{Ag}(k) + (1-C)\cdot\left(N_{Ag-Ag}\cdot\chi^{(N)}_{Ag-Ag}(k) + N_{Ag-Au}\cdot\chi^{(N)}_{Ag-Au}(k)\right) \quad (1)$$

where $(1 - C)$ - is the fraction of the silver atoms in Ag and AuAg nanoparticles. The small values of $(1 - C)$ (<0.1) and the choice of the upper boundary of the interval of wave-numbers $k_{\max} = 7$ Å^{-1} used for FT of $\chi_{\mathrm{Ag}}(k)$ according to [37] enabled to neglect the contribution of the second term in (1) in the R-range of the first peak of F(R), which corresponds dominantly to Ag–O contribution, and to obtain the value of C – percentage of silver interacting with oxygens. The value of $(1 - C)$, together with the results of XRF data analysis (which gives that the ratio of the total number of Ag atoms to Au atoms in each sample is Ag:Au ~ 13), enabled to estimate the upper boundary for the concentration of silver atoms (C_{Ag}) in bimetallic AuAg nanoparticles as:

$$C_{\mathrm{Ag,\ max}} \approx 1 - 1/(1 + 13\cdot(1 - C)) \quad (2)$$

This value is needed for determining the components (Au and Ag) distribution over the volume of mean AuAg nanoparticle in the construction of its cluster models.

Cluster modeling of atomic structure of AuAg nanoparticles was performed using the proposed technique [38,39] for visualization of the character of components distribution over the volume of mean AuAg particle in correspondence with the values of structural parameters derived from EXAFS. Besides of these structural parameters, generation of cluster model of mean bimetallic AuAg nanoparticle requires the values of the mean particles size $<D>$ and information of composition $<C_{\mathrm{Ag,\ max}}>$.

Simulations of SPR in optical extinction spectra of AuAg/glass samples, containing Ag, Au and AuAg nanoparticles of different structures, were performed using multi-spheres T-matrix approach [40], which allows to consider particles as a number of non-overlapping spheres, so that the core-shell particles were presented as a nested spheres. The dielectric functions of gold, silver and their alloys, which are required for the applied continuum-model simulations, were introduced in analytical form according to the study of Rioux et al. [41].

3. Results and discussion

3.1. Morphology and optical properties

Formation of metal nanoparticles by laser irradiation was first evidenced by STEM measurements. The representative TEM and STEM images for the gold coated and silver-doped glasses after laser irradiation with 5 and 200 pulses are presented in Fig. 1. All images indicate the presence of three types of nanoparticles: 1) small (4–10 nm) and 2) big (~40 nm) particles in the near-surface region, and 3) small particles (<5 nm) and their agglomerates located at larger distances (>50 nm) from the surface of glass. According to energy-dispersive X-ray spectroscopy (EDX) data, the latter particles (particles of type 3) are attributed to pure silver particles, which indicates that the penetration of gold atoms occurs only in the thin (<50 nm) layer of the glass surface. It must be noted that mixed AuAg composition was detected by EDX for both small and big particles in the near-surface region of glass (<50 nm) and the size distribution of these nanoparticles weakly depend upon the number of laser pulses, though some increase of the number of small particles was observed in TEM measurements, probably as a result of electron beam irradiation.

The presence of Au in the composition of both small and large nanoparticles is the consequence of the experimental technique for creation and implantation of Au particles from corresponding thin film using UV laser radiation [42,43]. Various experimental techniques for the formation of Au nanoparticles from a gold film of different thickness through the dewetting process have been developed [44,45] and it was revealed that the average size of the obtained particles depends on the thickness of the initial film: for a film thickness of ~5 nm (which corresponds in our technique to the film thickness after the first laser pulse with fluence 140 mJ/cm^2 [27]), the average particle size was determined as ~ 50 nm.

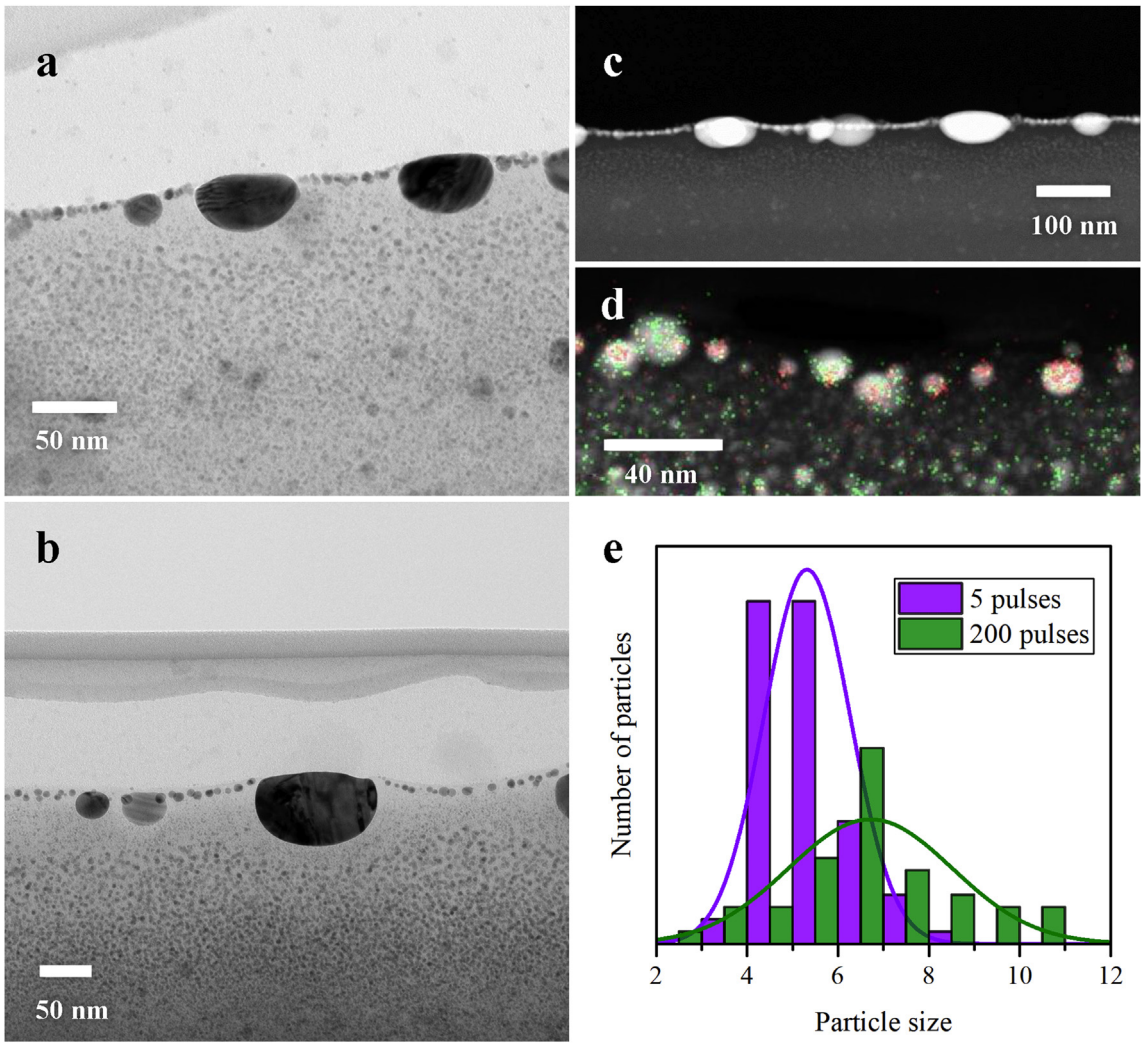

Fig. 1. Representative TEM images of the sample exposed to (a) 5 pulses and (b) 200 pulses. (c) STEM high-angle annular dark-field image of the sample exposed to 5 pulses. (d) STEM-EDX analysis of the sample after 200 pulses, where Au and Ag signals are marked by red and green respectively. (e) Size distribution of the small particles for the samples exposed to 5 (violet) and 200 (green) pulses. (For interpretation of the references to color in this figure legend, the reader is referred to the Web version of this article.)

However, in contrast to the above mentioned techniques, in our approach based on the use of nanosecond laser pulses, gold film does not undergo continuous thermal exposure. Under such a discrete-time treatment of the surface, the second laser pulse leads to the melting and fragmentation of the gold layer of thickness ~5 nm and as the result, in addition to the big particles (~40 nm), also a large number of small gold droplets or particles are formed as a consequence of dewetting process [46], which are implanted then into the glass by the few further laser pulses and are seen by TEM. The formation of gold particles of small and large sizes under few first laser pulses is schematically illustrated in Fig. 2 in agreement with the results of [27].

Optical extinction spectra of the Au/glass, Ag/glass and AuAg/glass samples, irradiated by different number of laser pulses are shown in Fig. 3. All spectra were subtracted by the basic glass (containing the silver ions in the case of Ag/glass and AuAg/glass samples). Comparison of spectra of as-prepared samples (Fig. S1 a–b) with those after cleaning with acetone (parts c – d) shows that the biggest differences after the cleaning procedure are observed for Au/glass samples (b, d), while the differences for AuAg/glass samples (a, c) are observed only for the cases of 1 and 2 laser pulses. This can be explained by the presence of silver ions, which enhance the absorption of laser irradiation and as a consequence, the melting of the glass surface which provides better implantation of the gold particles into the AuAg/glass samples. In Au/glass samples, to achieve the same degree of implantation a lot more laser pulses required. For AuAg/glass samples prepared by 1 and 2 pulses, the differences in spectra of samples after cleaning by acetone and without it are expectable since after the first pulse, the disintegration of the gold layer is observed, and after the second pulse the first nanoparticles are formed without implantation into the surface, and therefore the acetone cleaning procedure removes almost all gold from the surfaces of AuAg/glasses. For Ag/glass samples no difference is observed, since the silver ions are initially incorporated into the glass and the cleaning procedure does not affect the samples.

Position of SPR in the spectra of AuAg/glass samples (Fig. 3c) is shifting with the increasing of number of pulses from its position in spectra of Au/glass samples to the position in spectra of Ag/glass. However, these changes cannot be reproduced by simple linear combination of corresponding spectra for Au/glass and Ag/glass samples, indicating a possible alloying of gold and silver.

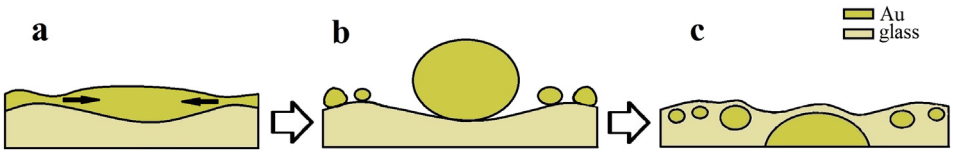

Fig. 2. Schematic illustration of the formation of a large and small gold particles from the thin gold film of ~5 nm remaining after the first pulse (a), the second (b) and few further pulses of laser irradiation of the glass (c) according to [27]. (For interpretation of the references to color in this figure legend, the reader is referred to the Web version of this article.)

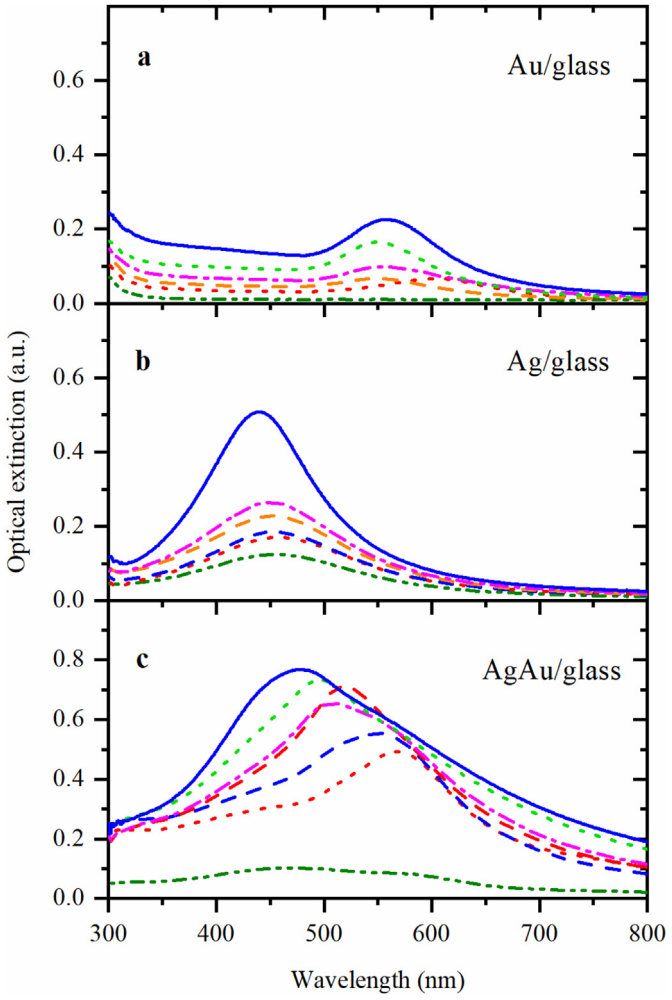

Fig. 3. Optical extinction spectra of samples Au/glass (a), Ag/glass (b) and AuAg/glass (c). Samples were obtained using laser irradiation with different number of pulses: 2 pulses (olive dash-dot-doted curve), 5 pulses (red doted), 10 pulses (blue dashed curve), 50 pulses (red dashed curve), 100 pulses (magenta dash-doted curve), 200 pulses (green doted curve), 1000 pulses (blue solid curve). (For interpretation of the references to color in this figure legend, the reader is referred to the Web version of this article.)

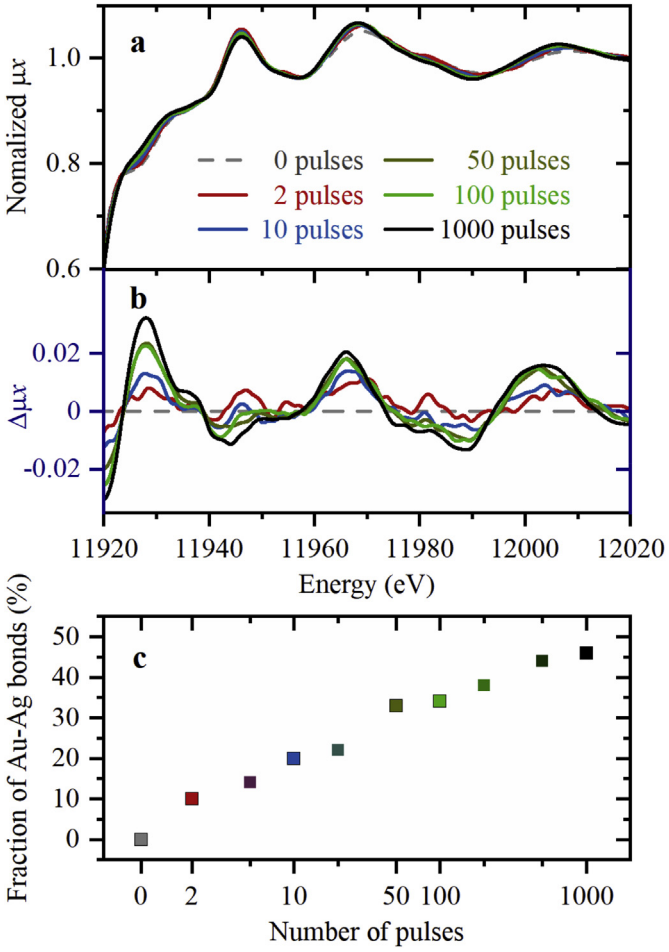

Fig. 4. Au L_3-XANES spectra (a) of the silver doped and gold coated glass irradiated by different number of laser pulses (colored curves): from 0 (dashed black line) to 1000 (solid black line) and corresponding difference spectra (b). Part (c) shows the evolution of Au–Ag contribution to XANES spectra obtained by the fitting. (For interpretation of the references to color in this figure legend, the reader is referred to the Web version of this article.)

3.2. XAFS study of bimetallic AuAg nanoparticles in AuAg/glass samples

Monotonic changes with the increasing number of the applied laser pulses were observed in Au L_3-edge XANES spectra of the studied AuAg/glass samples (Fig. 4a). These changes can be best appreciated in difference XANES spectra (Fig. 4b) constructed by subtraction of the spectrum of non-irradiated gold-coated glass from each XANES spectrum. This difference is observed only for AuAg/glass samples, and not for Au/glass, evidencing the formation of bimetallic nanoparticles. To evaluate the degree of Ag–Au alloying, the experimental difference spectra were fitted by the theoretical ones. At the first step, two spectra were calculated for the two extreme cases: a) pure gold atomic cluster and b) single gold atom in the center of the silver cluster. Then, a spectrum for any given fraction of Au–Ag/Au–Au from 0 to 100% can be obtained as a liner combination of the two calculated boundary structural states. The parameter of this combination was then varied to obtain the minimum of the root-mean-square deviation between experimental and theoretical difference spectrum. The obtained results are presented in Fig. 4c. The interatomic distance was not varied because the difference in the length of Au–Au and Au–Ag bonds is negligible and does not affect the near-edge region of the spectra.

The evolution of Au–Ag fraction upon the number of laser

pulses, plotted in a logarithmic scale, has a monotonic and almost linear behavior. The stepwise changes are observed between the non-irradiated sample and sample after 2 laser pulses, and between 20 and 50 pulses, which correlates with the regions where the biggest changes of SPR position were observed in the corresponding optical spectra (Fig. 3). For the big number of pulses, the fraction of Au–Ag bonds is approaching 50%, which indicates the formation of AuAg solid solution with approximately equal number of Ag and Au atoms in the NPs. This means that after application of 2 laser pulses, the dominating are pure gold nanoparticles, with small fraction of Au–Ag contribution, and after 1000 pulses, we have the structure of a disordered solid solution of gold and silver in all particles. The lower fraction of Au–Ag bonds in AuAg/glass samples at the lower number of pulses can originate either from small amount of Ag in the Au-containing particles (which is the consequence of the dominant existence of separate Ag and Au nanoparticles), or from the particular distribution of the Ag and Au atoms in the volume of AuAg particle which differ from the ideal solid solution (e.g. core-shell structures). The further study of the components (Au and Ag) distribution in AuAg nanoparticles was performed by EXAFS.

Fourier-transforms |F(*R*)| of experimental Ag *K*-edge EXAFS in AuAg/glass samples presented in Fig. 5a show the decreasing of the first peak (at ~ 1.5 Å), attributed mainly to Ag–O bonds, and increasing of the second peak (at ~ 3.0 Å), attributed mainly to Ag–Ag and Ag–Au bonds, with the increasing number of laser pulses used for samples creation. The decreasing of the first peak indicates that part of Ag-ions in the glass matrix are reduced to Ag-atoms forming Ag and AuAg nanoparticles. Analysis of |*F*(*R*)| of experimental Au L_3-edge EXAFS of Fig. 5b shows the absence of features attributed to Au–O bonds (in contrast to Ag–O ones in Fig. 5a), which can be explained by the relatively large sizes of Au and AuAg particles (according to TEM) from the one side and by the probable partly coating of their surface by Ag atoms, which can be expected from EDX. As a consequence, one can neglect the Au–O contributions into |*F*(*R*)| of Au L_3-EXAFS within the R-range of Au–Au or Au–Ag bonds of the absorbing Au-atom and consider these functions as the direct source of information on the number and structural parameters of Au–Au and Au–Ag bonds. |F(*R*)| presented in Fig. 5b indicate the decrease of the first peak at ~ 2.3 Å and simultaneous increase of the second peak at ~ 3.0 Å with the increase of the number of pulses. Comparison of |F(*R*)| of theoretical functions $k{\cdot}\chi(k)$ calculated for atomic pairs $(Au)_{absorbing\ atom} - (Au)_{neighboring\ atom}$ and $(Au)_{absorbing\ atom} - (Ag)_{neighboring\ atom}$ presented in Fig. 5c elucidate that the observed monotonic changes in the magnitudes and positions of the first and the second peaks of |F(*R*)| in Fig. 5b reflect the increasing of the number of Au–Ag bonds and decreasing of Au–Au bonds with the number of laser pulses, similarly as was observed from XANES region. Fig. 5b shows also that in the extended *R*-range (beginning from ~3.5 Å), the features of |F(*R*)| of AuAg/glass samples at different number of pulses repeat the features of |F(*R*)| for non-irradiated AuAg/glass sample (or Au foil) which means that the local atomic structure of the Au atoms in nanoparticles is close to *fcc*.

These qualitative conclusions were confirmed by the results of the fitting of F(*R*) of the experimental Au L_3-edge EXAFS, which was performed using the models of Au local atomic structures in AuAg/glass samples. In bimetallic AuAg nanoparticles, each Au atom can be surrounded either exclusively by Au or Ag atoms, or by both of them, depending on atomic composition of the particles and distribution of Au and Ag atoms in the particle's volume. All possible cases can be combined within the models for Au local structures in which some of the first neighbors of the absorbing atoms are gold atoms and other are silver atoms. The contributions in $\chi(k)$ which correspond to photoelectron scattering processes on a one nearest

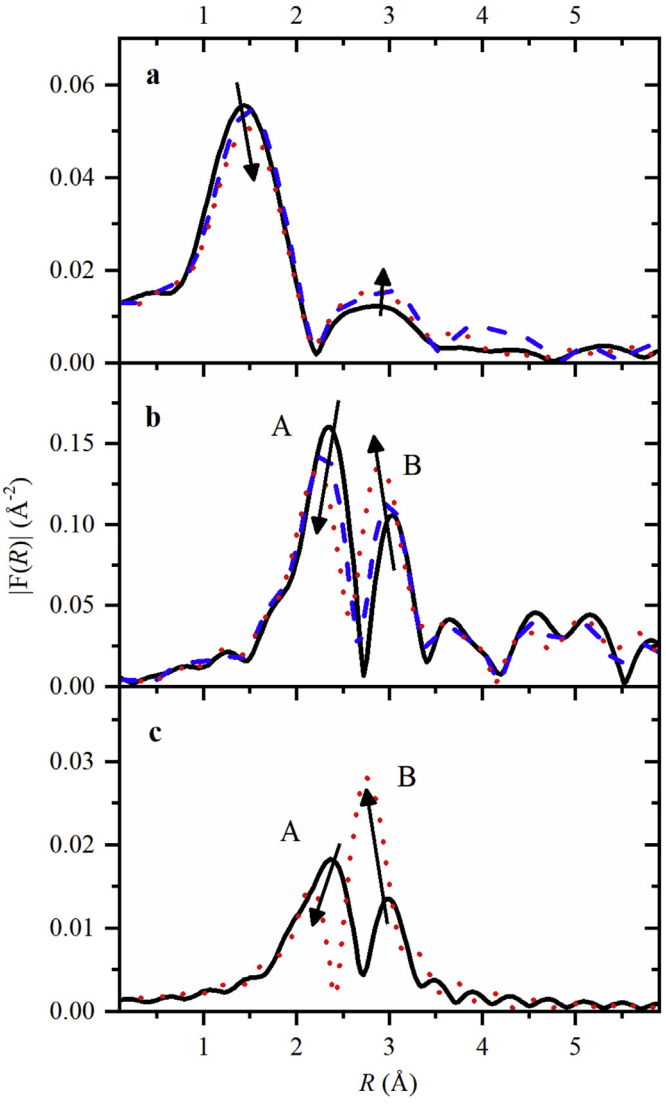

Fig. 5. FT magnitudes |F(*R*)| of oscillatory functions $k{\cdot}\chi(k)$ of experimental Ag *K*-edge (a) and Au L_3-edge EXAFS (b) for AuAg/glass samples: non-irradiated (solid black curve), irradiated by 10 (dash blue curves) and 1000 (dot red curves) laser pulses. Part (c) compares |F(*R*)| of theoretical functions $k{\cdot}\chi(k)$ calculated for atomic pairs: $(Au)_{absorbing\ atom} - (Au)_{neighboring\ atom}$ (solid black curve) and $(Au)_{absorbing\ atom} - (Ag)_{neighboring\ atom}$ (dash red curve). (For interpretation of the references to color in this figure legend, the reader is referred to the Web version of this article.)

atom of a specific type are denoted as $\chi_{Au\text{-}Au}$ and $\chi_{Au\text{-}Ag}$ where the first label in subscript indicates the absorbing Au atom and the second label – the scattering one. Neglecting the discussed above effect of Au–O interactions and denoting the contribution of the scattering processes on the second and more distant shells, and the multiple-scattering processes as $\tilde{\chi}_{Au}$ for absorbing Au atom, the oscillatory parts $\chi_{Au}(k)$ of Au L_3-EXAFS can be written as:

$$\chi_{Au}(k) = N_{Au-Au}\cdot\chi_{Au-Au}(k) + N_{Au-Ag}\cdot\chi_{Au-Ag}(k) + \tilde{\chi}_{Au} \qquad (3)$$

where N_{Au-Au}, N_{Au-Ag} – are the numbers of atoms of a specific type in the first coordination shell of the absorbing Au atom (partial coordination numbers) averaged over all absorbing Au atoms of all nanoparticles.

Determination of the structural parameters for the nearest neighbors of the absorbing Au atom in the studied nanoparticles using FT of EXAFS enables to neglect the contribution of the last

term $\tilde{\chi}_{Au}$ in Eq. (3). This can be done because of the reduction of contribution of the second and more distant shells in relation to the nearest neighbors one in *fcc*-like structure within the *R*-range of the nearest neighbors of the absorbing Au, which was confirmed by the model calculations [47]. The fit of F(*R*) of Au L_3-edge EXAFS in the studied AuAg/glass samples was performed by such a "nearest neighbors" approximation of Eq. (3) and using the technique of [29,36] for reducing the effect of correlation between fitting parameters on the obtained values of structural parameters. To diminish the number of variables, the reduction factor [48] was fixed to its value $S_0^2(\mathrm{Au}) = 0.87$ obtained for the reference Au thin film. The independently varied parameters were: partial coordination numbers $N_{\mathrm{Au-Au}}$, $N_{\mathrm{Au-Ag}}$, corresponding Debye-Waller (DW) parameters ($\sigma^2_{\mathrm{Au-Au}}$, $\sigma^2_{\mathrm{Au-Ag}}$) and interatomic distances ($R_{\mathrm{Au\text{-}Au}}$, $R_{\mathrm{Au\text{-}Ag}}$). The obtained values of mean Au–Au and Au–Ag structural parameters for the samples prepared by different number of laser pulses are presented in Table 1. As can be seen, the obtained values of the DW parameters σ^2 are quite reasonable for the room temperature [49] which indicates that the fit model (3) enabled to account for Au local structures in the AuAg/glass samples. It must be mentioned that the values of structural parameters in the samples obtained by the small number of laser pulses are determined with bigger error due to the low Au–Ag contributions.

TEM data suggest that there are two types of particles in AuAg/glass sample containing Au atoms: small particles with a size of about 5–10 nm and large particles of ~40 nm in size. According to the principles of EXAFS signal formation, the values of structural parameters presented in Table 1 correspond to the mean AuAg nanoparticle in AuAg/glass sample with the weighted average value of size (*D*) and the average ratio of components Ag:Au. Pure Au nanoparticles, which can be formed in addition to bimetallic ones, can be included into this average bimetallic model and correspond to the values $C_{\mathrm{Au}} = 1.0$, $C_{\mathrm{Ag}} = 0.0$ (C_{Au} and C_{Ag} are the fractions of gold and silver atoms in the mean AuAg particle, respectively). Fig. 6 shows the dependences of the values of partial coordination numbers of Table 1 and the total coordination number $N_{\mathrm{Au}} = N_{\mathrm{Au-Au}} + N_{\mathrm{Au-Ag}}$ of the absorbing Au atom in the mean AuAg particle upon the number of laser pulses used for preparation of AuAg/glass samples.

From the available TEM data, the ratio of the small (5–10 nm) to large (~40 nm) particles cannot be precisely obtained. Besides, an estimate of the mean particle size <*D*> in AuAg/glass samples at different number of pulses by the processing of X-ray diffraction (XRD) data gave the values of <*D*> ~ 15–20 nm for the amount of Ag and AuAg nanoparticles and hence, there is an ambiguity in the value of mean size of AuAg particles. However, for the sample prepared by small number of pulses (2 pulses) the experimental Au L_3-EXAFS spectrum differ from that for the non-irradiated sample coated with a thin gold film (0 pulses) (Fig. S2). This means that the small particles, already existed in the sample at low number of pulses, significantly contribute into the formation of the EXAFS signal. In this case, the largest value of the total coordination

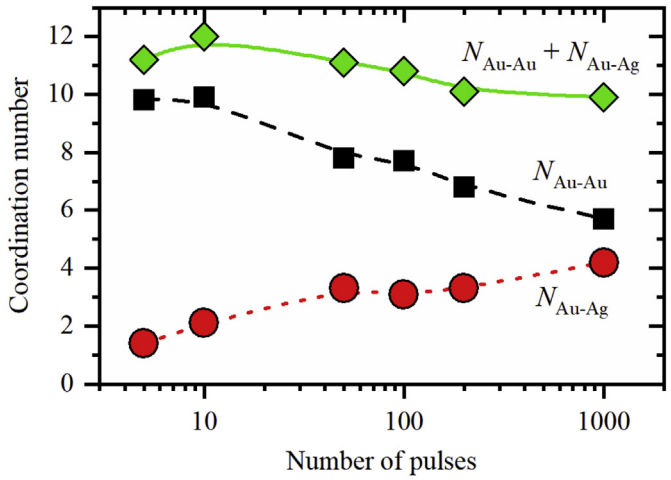

Fig. 6. Dependencies of partial coordination numbers $N_{\mathrm{Au-Au}}$ (dashed black curve), $N_{\mathrm{Au-Ag}}$ (dotted red curve) and the total coordination number $N_{\mathrm{Au}} = N_{\mathrm{Au-Au}} + N_{\mathrm{Au-Ag}}$ (solid green curve) of the absorbing Au atom in AuAg/glass samples upon the number of laser pulses used for the samples preparing. (For interpretation of the references to color in this figure legend, the reader is referred to the Web version of this article.)

number $N_{\mathrm{Au}} \approx 12$ of the absorbing Au atom in the sample with 10 laser pulses means that the Au atoms are dominantly located in the volume of AuAg nanoparticle and the most plausible model of mean particle for this sample is the core-shell model with the shell consisted dominantly of Ag atoms (often used notation for this core-shell architecture is Au@Ag). Further increase of the number of laser pulses leads to the decrease of the total coordination number N_{Au} indicating that the core-shell architecture is destroyed due to enhancing interdiffusion of silver atoms of the shell and gold atoms of the core, thus forming the structure of disordered solid solution, which is completely formed at 1000 laser pulses in agreement with the results of the analysis of Au L_3-edge XANES.

An estimate of the upper boundary for the percentage of silver atoms, attributed to Ag and AuAg particles, performed by the prescription of Sec.2.2 for the processing of Ag *K*-edge EXAFS and using Eq. (2) with the ratio of the total number of Ag to Au atoms in each sample determined by XRF, enabled to obtain the following maximum values for the concentration of silver atoms in bimetallic AuAg nanoparticles: $(C_{\mathrm{Ag}})_{\mathrm{max}} = 44\%$, 48% and 57% for AuAg/glass samples prepared by 50, 100 and 1000 laser pulses respectively.

3.3. Visualization of atomic structure of bimetallic AuAg nanoparticles

The EXAFS-derived values of structural parameters reported in Table 1 for the nearest neighbors of Au atoms in the AuAg/glass samples enables to make only indirect conclusions on the atomic structure of the formed nanoparticles. Meanwhile, to determine the

Table 1
Structural parameters of Au–Au and Au–Ag bonds in AuAg/glass samples, prepared by different number of laser pulses.

Pulses number	Au–Au			Au–Ag		
	$R_{\mathrm{Au-Au}}$, Å	$N_{\mathrm{Au-Au}}$	σ^2(Au–Au), Å^2	$R_{\mathrm{Au-Ag}}$, Å	$N_{\mathrm{Au-Ag}}$	σ^2(Au–Ag), Å^2
2	2.88 ± 0.01	10.0 ± 0.7	0.009 ± 0.001	2.90 ± 0.03	0.7 ± 0.6	0.010 ± 0.002
5	2.88 ± 0.01	9.8 ± 0.7	0.008 ± 0.001	2.89 ± 0.03	1.4 ± 0.6	0.010 ± 0.002
10	2.88 ± 0.01	9.9 ± 0.7	0.010 ± 0.001	2.90 ± 0.01	2.1 ± 0.6	0.011 ± 0.001
50	2.88 ± 0.01	7.8 ± 0.5	0.008 ± 0.001	2.88 ± 0.01	3.1 ± 0.5	0.009 ± 0.001
100	2.88 ± 0.01	7.7 ± 0.5	0.008 ± 0.001	2.88 ± 0.01	3.2 ± 0.5	0.008 ± 0.001
200	2.88 ± 0.01	6.8 ± 0.5	0.008 ± 0.001	2.88 ± 0.01	3.3 ± 0.5	0.007 ± 0.001
1000	2.88 ± 0.01	5.7 ± 0.4	0.008 ± 0.001	2.88 ± 0.01	4.2 ± 0.4	0.009 ± 0.001

relationship between synthesis conditions – atomic structure – optical performances of these materials, it is necessary to visualize the character of components (Au and Ag) distribution over the volume of mean AuAg nanoparticle in correspondence with the values of structural parameters derived from EXAFS. In particular, it is decisive to reveal the synthesis conditions which provide the excess of Ag atoms in the near-surface region of particle: formation of silver shell, its thickness, continuity, etc.

To suggest models of mean AuAg nanoparticle in each AuAg/glass sample, the method of atomic cluster simulation [38] was applied, in which the radial probability function with four varying parameters was used so as to match the values of the EXAFS derived structural parameters. Note, that monometallic gold particles are effectively accounted in a model of bimetallic AuAg particles and are not considered separately. However, this approach can lead to an overestimation of gold content in the cluster model of mean AuAg nanoparticle retaining qualitative conclusions on the formation of core-shell or alloy architecture. As was mentioned in Sec. 2.2, generation of cluster model of mean bimetallic AuAg nanoparticle in the sample requires also the knowledge of the mean particles size <*D*> and the mean percentage C_{Ag} of Ag atoms in the mean nanoparticle. Due to the mentioned ambiguities in the determination of these parameters, it is impossible to suggest the single-valued model of bimetallic particles and therefore, the reasonable way for the cluster modeling of AuAg nanoparticles is to generate AuAg *fcc* clusters of different sizes *D* and use one more varied parameter C_{Ag} for each cluster of the considered size, choosing the most plausible models by additional condition $C_{Ag} \leq C_{Ag,\,max}$, where $C_{Ag,\,max}$ was determined according to Sec. 2.2. By this scheme, the most plausible cluster models of AuAg nanoparticles, which can be expected in AuAg/glass sample irradiated by a specific number of laser pulses, were obtained. Fig. 7 show the cross-sections of such cluster models of bimetallic AuAg NPs in AuAg/glass samples irradiated by10, 50, 100 and 1000 laser pulses (the obtained values of C_{Ag} for each model are also presented).

As can be seen, at low number of laser pulses (~10) there is an excess of Ag content in the near surface region of clusters with different sizes and therefore one can expect that the core-shell architecture of AuAg nanoparticles with Au-core and Ag-shell (Au@Ag) is probably dominant for the allowed values of C_{Ag}, and does not depend on the considered particles sizes *D*. However, the thickness of Ag-shell and its continuity strongly depend upon the values of C_{Ag} and *D*. With the increasing of pulses number (50 pulses and more), the interdiffusion of Ag atoms of shell and Au atoms of core enhances which leads to the smearing of the core-shell architecture and the formation of the structure of disordered solid solution in agreement with the above results of the XANES analysis. The increase of C_{Ag} in the obtained cluster models of AuAg particles with the number of pulses seems reasonable since laser irradiation continues reducing of silver ions into neutral state, while the number of gold atoms doesn't increase. One more conclusion which can be made from the performed cluster modeling is that the EXAFS signal in AuAg/glass samples at low number (10) of pulses can be formed by AuAg nanoparticles with mean sizes of ~7–20 nm while at the large number of pulses (50 and more) – by the particles with mean sizes of 7–10 nm. In the last case, the effect of the presence of the few large AuAg particles (of sizes ~ 40–50 nm) together with the main amount of the small ones in AuAg/glass samples on the formation of the EXAFS requires additional study.

3.4. Optical extinction spectra of AuAg/glass samples

Characteristics of SPR in optical extinction spectra of AuAg/glass samples must be sensitive to the particles architecture [21], to size distribution and to the spatial arrangement of particles in their aggregates [50]. The aim of this section is to show that the revealed architectures and percentage composition of AuAg nanoparticles are suitable for the description of the observed optical extinction spectra or, in other words, the observed optical properties are not in contradiction with the proposed structure models. With this purpose, the simple calculations of SPR spectra were performed using multi-spheres T-matrix approach [40]. The obtained results have qualitative character since only contributions from single particles

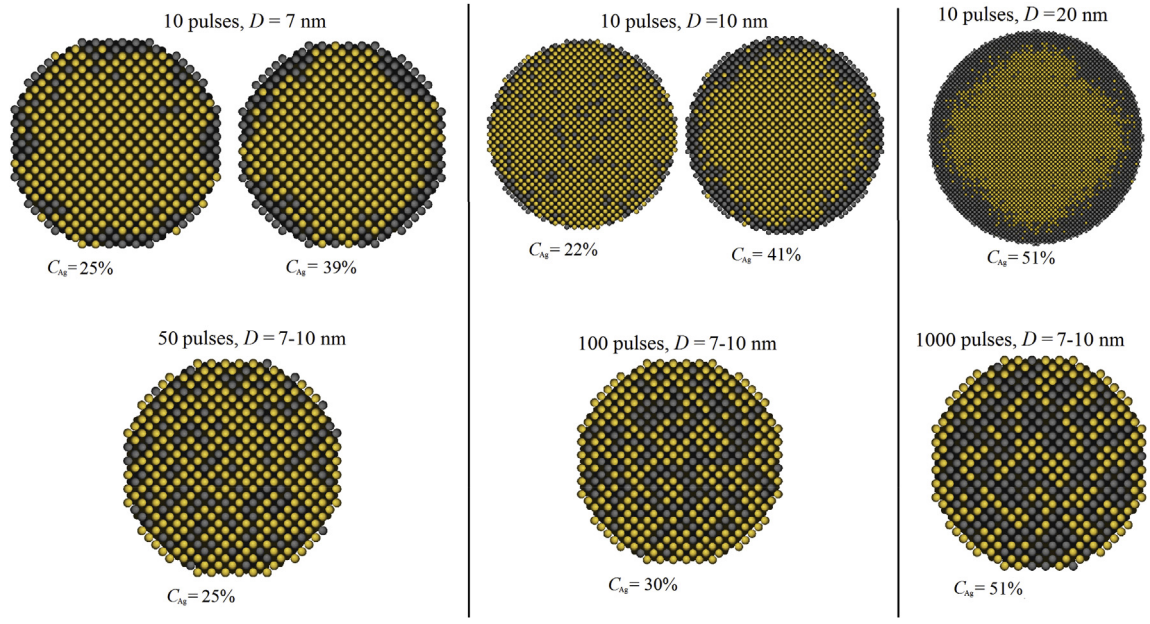

Fig. 7. Cross-sections of the atomic cluster models of bimetallic AuAg nanoparticles in AuAg/glass samples irradiated by 10, 50, 100 and 1000 pulses. Models were obtained by the technique [38] using additional parameter C_{Ag} which was varied for the atomic clusters of different sizes. (Au and Ag atoms are shown as yellow and black balls, respectively). (For interpretation of the references to color in this figure legend, the reader is referred to the Web version of this article.)

with the core-shell or disordered alloy architecture were considered, neglecting the size dispersion and particles interactions or aggregation effects, which could be significant for optical spectra description [50]. The dielectric functions of silver, gold and their alloys were taken in analytical form [41] which reproduces the observed optical properties of bulk alloy.

Fig. 8 shows the possible decomposition of experimental SPR spectra of AuAg/glass samples obtained after irradiation by 10 (Fig. 8a) and 200 (Fig. 8b) laser pulses. In both experimental spectra one can see the contribution of silver particles of sizes ~7 nm, which is in agreement with TEM data. However, the features of the main SPR peaks require consideration of the AuAg particles. Thus, for AuAg/glass sample at 10 pulses the main peak features can be attributed to the core-shell AuAg particles (Au-core, Ag-shell) with C_{Ag} ~ 25% and two different sizes of ~10 nm and of ~40 nm, which qualitatively agrees with the above reported TEM data and structural models proposed from EXAFS. It must be noted, that the same SPR position can be obtained using pure gold particles of sizes ~30 nm instead of Au@Ag nanoparticles, which indicates on the ambiguity in the performed decomposition of the experimental optical spectra.

The spectrum of AuAg/glass sample at 200 pulses (Fig. 8b) shows that SPR position is shifted by ~ 50 nm towards lower wavelengths which can be explained according to the EXAFS results by the presence of small (~7–10 nm) AuAg particles with the structure of disordered alloy and higher silver content (~30%) on the background of contributions of pure silver particles of size ~ 10 nm and of a few (according to TEM and EXAFS) large AuAg particles, also with alloyed structure and size ~ 50 nm. Unlike to the AuAg/glass sample at 10 pulses, the suggested decomposition of SPR features in the spectrum of sample at 200 pulses seems single-valued.

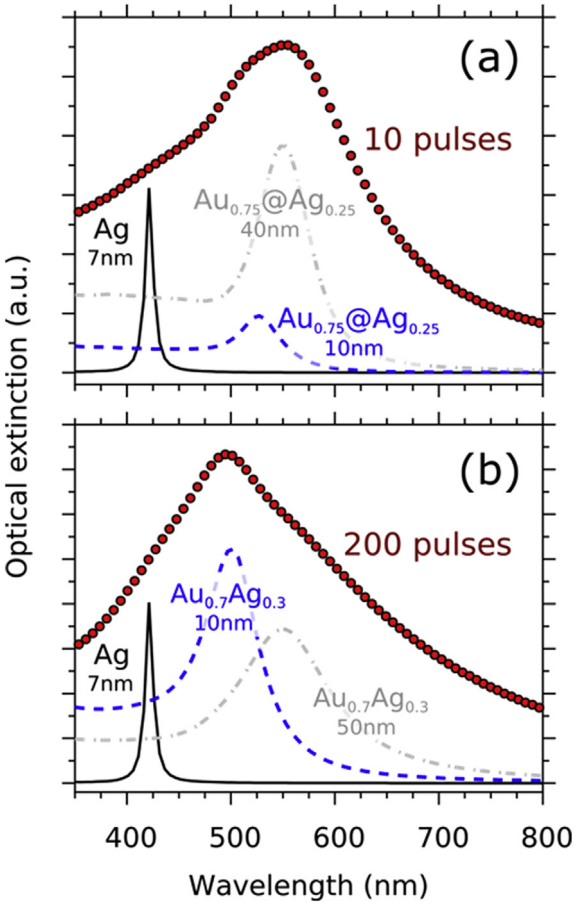

Fig. 8. Possible decompositions of SPR in experimental optical extinction spectra (red dots) of AuAg/glass samples, obtained after irradiation by 10 (a) and 200 (b) laser pulses, into a number of theoretical spectra of single particles, calculated for different architectures, sizes and compositions of particles. In both panels: 7 nm Ag particle (solid lines); part (a): 10 nm core(Au)-shell(Ag) particle with 25 at.% Ag (dashed line), 40 nm core(Au)-shell(Ag) particle with 25 at.% Ag (dash-dot line); part (b): 10 nm AuAg alloyed particle with 30 at.% Ag (dashes), 50 nm AuAg alloyed particle with 30 at.% Ag (dash-dot line). (For interpretation of the references to color in this figure legend, the reader is referred to the Web version of this article.)

Quantitative analysis of the experimental optical extinction spectra through decomposition of SPR into several most plausible contributions requires accounting for interparticles interactions. For such analysis, further development of the approach, proposed in Ref. [50] for monometallic particles, to the bimetallic AuAg ones must be performed.

4. Conclusions

The results of the performed study can be summarized in the following conclusions:

- laser irradiation by ArF-excimer laser (193 nm) of the glass surface preliminary prepared via $Ag^{+} \leftrightarrow Na^{+}$ ion exchange and then sputter coated with a thin gold layer, enabled to create both bimetallic AuAg and monometallic Au and Ag nanoparticles in the near-surface region of AuAg/glass sample;
- even after two laser pulses, two types of bimetallic AuAg nanoparticles are formed in the near-surface region (<50 nm) of glass: small particles of sizes 5–10 nm and big ones ~ 40 nm. Meanwhile, at the deeper regions of glass (>50 nm from the surface) only pure silver particles of sizes ~ 7 nm are formed;
- characteristics of SPR in optical extinction spectra of the obtained AuAg/glass samples strongly depend upon the number of laser pulses used for samples preparing: thus, the wavelength position of SPR is shifted by ~ 100 nm to the lower values with the increasing of pulses number from 5 to 1000. This shift cannot be reproduced within simple linear combination of corresponding SPR in Au/glass and Ag/glass samples;
- under laser irradiation, almost all gold particles were implanted into the glass by applying only few laser pulses (5–10) due to the increased glass absorption as a consequence of the presence of silver in the near-surface region of samples. Therefore, the ratio of atoms Au:Ag in each sample remains stable under applying further laser pulses up to 1000 and the upper boundary of concentration of silver atoms in AuAg nanoparticles was estimated as a function of the number of laser pulses used for preparing of AuAg/glass samples. Laser irradiation of samples leads to the increasing of silver content in AuAg nanoparticles due to decrease of the number of silver ions in glass;
- at the low number of laser pulses (~10) the created AuAg nanoparticles have dominantly the core-shell architecture with Au-core and Ag-shell. Cluster modeling shows that this architecture is stable for the particles with mean sizes of 7–20 nm. However, the thickness of the silver shell and its continuity depend upon the percentage of silver atoms in the mean AuAg nanoparticle;
- with the increasing of the number of pulses (50 pulses and more) the core-shell architecture of AuAg particles becomes smeared which leads to the formation of the structure of disordered solid solution in bimetallic AuAg nanoparticles with mean sizes of 7–10 nm;
- simulations of optical extinction spectra of AuAg/glass samples using two different architectures of AuAg nanoparticles provided by XAFS, show that under the considered percentage of

silver atoms in mean particle, the structure of disordered alloy provides even more strong dependence of SPR position (shift by ~ 50–60 nm for samples at 10 and 200 pulses) upon the considered particles sizes than the desired core-shell architecture. However, these dependences require further study taking into account size dispersion and interparticles interaction, which is beyond the scope of the present work.

Acknowledgements

The work was supported by DFG-RFBR project (DFG No DU 214/14-1, RFBR No 14-02-91334). V.V.S., L.A.A., A.V.S., S.Yu.K and L.A.B. acknowledge the Southern Federal University for the financial support. Authors would like to thank Olivier Mathon, Kirill Lomachenko, and Alessandro Longo for their help during XAFS measurements at BM23 and BM26A beamlines at ESRF, proposals MA-3438 and CH-5046.

Appendix A. Supplementary data

Supplementary data related to this article can be found at https://doi.org/10.1016/j.jallcom.2018.07.183.

References

[1] M.C. Daniel, D. Astruc, Gold nanoparticles: assembly, supramolecular chemistry, quantum-size related properties and applications toward biology, catalysis and nanotechnology, Chem. Rev. 104 (2004) 293–346, https://doi.org/10.1021/cr030698.
[2] S. Linic, P. Christopher, D.B. Ingram, Plasmonic-metal nanostructures for efficient conversion of solar to chemical energy, Nat. Mater. 10 (2011) 911–921, https://doi.org/10.1038/nmat3151.
[3] P.V. Kamat, Photophysical, photochemical and photocatalytic aspects of metal nanoparticles, J. Phys. Chem. B 106 (2002) 7729–7744, https://doi.org/10.1021/jp0209289.
[4] G.G. Li, Y. Lin, H. Wang, Residual silver remarkably enhances electrocatalytic activity and durability of dealloyed gold nanosponge particles, Nano Lett. 16 (2016) 7248–7253, https://doi.org/10.1021/acs.nanolett.6b03685.
[5] A.V. Okhokhonin, S.Y. Saraeva, A.I. Matern, A.N. Kozitsina, Enzymeless determination of cholesterol using gold and silver nanoparticles as electrocatalysts, J. Anal. Chem. 72 (2017) 354–361, https://doi.org/10.1134/S1061934817040116.
[6] K. Saha, S.S. Agasti, C. Kim, X. Li, V.M. Rotello, Gold nanoparticles in chemical and biological sensing, Chem. Rev. 112 (2012) 2739–2779, https://doi.org/10.1021/cr2001178.
[7] H. Tao, Y. Lin, J. Yan, J. Di, A plasmonic mercury sensor based on silver–gold alloy nanoparticles electrodeposited on indium tin oxide glass, Electrochem. Commun. 40 (2014) 75–79, https://doi.org/10.1016/j.elecom.2014.01.002.
[8] L. Sun, Q. Li, W. Tang, J. Di, Y. Wu, The use of gold-silver core-shell nanorods self-assembled on a glass substrate can substantially improve the performance of plasmonic affinity biosensors, Microchim. Acta. 181 (2014) 1991–1997, https://doi.org/10.1007/s00604-014-1285-7.
[9] P.K. Jain, X. Huang, I.H. El-Sayed, M.A. El-Sayed, Noble metals on the nanoscale: optical and photothermal properties and some applications in imaging, sensing, biology, and medicine, Acc. Chem. Res. 41 (2008) 1578–1586, https://doi.org/10.1021/ar7002804.
[10] T. Stuchinskaya, M. Moreno, M.J. Cook, D.R. Edwards, D.A. Russell, Targeted photodynamic therapy of breast cancer cells using antibody–phthalocyanine–gold nanoparticle conjugates, Photochem. Photobiol. Sci. 10 (2011) 822, https://doi.org/10.1039/c1pp05014a.
[11] S.D. Brown, P. Nativo, J.-A. Smith, D. Stirling, P.R. Edwards, B. Venugopal, et al., Gold nanoparticles for the improved anticancer drug delivery of the active component of oxaliplatin, J. Am. Chem. Soc. 132 (2010) 4678–4684, https://doi.org/10.1021/ja908117a.
[12] W.L. Barnes, A. Dereux, T.W. Ebbesen, Surface plasmon subwavelength optics, Nature 424 (2003) 824–830, https://doi.org/10.1038/nature01937.
[13] S. Eustis, M.A. El-Sayed, Why gold nanoparticles are more precious than pretty gold: noble metal surface plasmon resonance and its enhancement of the radiative and nonradiative properties of nanocrystals of different shapes, Chem. Soc. Rev. 35 (2006) 209–217, https://doi.org/10.1039/B514191E.
[14] P. Mulvaney, Surface plasmon spectroscopy of nanosized metal particles, Langmuir 12 (1996) 788–800, https://doi.org/10.1021/la9502711.
[15] S. Link, M.A. El-Sayed, Size and temperature dependence of the plasmon absorption of colloidal gold nanoparticles, J. Phys. Chem. B 103 (1999) 4212–4217, https://doi.org/10.1021/JP984796O.
[16] P.K. Jain, K.S. Lee, I.H. El-Sayed, M.A. El-Sayed, Calculated absorption and scattering properties of gold nanoparticles of different size, shape, and composition: applications in biological imaging and biomedicine, J. Phys. Chem. B 110 (2006) 7238–7248, https://doi.org/10.1021/jp057170o.
[17] H. Ditlbacher, J.R. Krenn, B. Lamprecht, A. Leitner, F.R. Aussenegg, Spectrally coded optical data storage by metal nanoparticles, Opt. Lett. 25 (2000) 563, https://doi.org/10.1364/OL.25.000563.
[18] S.M. Hamidi, S. Behjati, Large area multi-channel plasmonic absorber based on the touching triangular dimers fabricated by angle controlled colloidal nanolithography, Optic Laser. Technol. 99 (2018) 203–213, https://doi.org/10.1016/j.optlastec.2017.09.004.
[19] C. Louis, S. Roux, G. Ledoux, L. Lemelle, P. Gillet, O. Tillement, et al., Gold nanoantennas for increasing luminescence, Adv. Mater. 16 (2004) 2163–2166, https://doi.org/10.1002/adma.200400299.
[20] G. Gouesbet, G. Grehan, Generalized Lorenz-Mie theory for assemblies of spheres and aggregates, J. Opt. A Pure Appl. Opt. 1 (1999) 706–712, https://doi.org/10.1088/1464-4258/1/6/309.
[21] C. Zhang, B.-Q. Chen, Z.-Y. Li, Y. Xia, Y.-G. Chen, Surface plasmon resonance in bimetallic core–shell nanoparticles, J. Phys. Chem. C 119 (2015) 16836–16845, https://doi.org/10.1021/acs.jpcc.5b04232.
[22] W. Schärtl, Crosslinked spherical nanoparticles with core-shell topology, Adv. Mater. 12 (2000) 1899–1908, https://doi.org/10.1002/1521-4095(200012)12:24<1899::AID-ADMA1899>3.0.CO;2-T.
[23] J. Deng, J. Du, Y. Wang, Y. Tu, J. Di, Synthesis of ultrathin silver shell on gold core for reducing substrate effect of LSPR sensor, Electrochem. Commun. 13 (2011) 1517–1520, https://doi.org/10.1016/j.elecom.2011.10.010.
[24] P. Dong, Y. Lin, J. Deng, J. Di, Ultrathin gold-shell coated silver nanoparticles onto a glass platform for improvement of plasmonic sensors, ACS Appl. Mater. Interfaces 5 (2013) 2392–2399, https://doi.org/10.1021/am4004254.
[25] M. Dubiel, M. Heinz, M. Stiebing, J. Meinertz, J. Ihlemann, T. Rainer, Generation and characterization of plasmonic nanostructures in glass surfaces by means of excimer and solid state laser irradiation, in: A.D. Boardman (Ed.), SPIE Nanosci. + Eng, International Society for Optics and Photonics, 2014, p. 91631M, https://doi.org/10.1117/12.2061034.
[26] M. Heinz, V.V. Srabionyan, A.L. Bugaev, V.V. Pryadchenko, E.V. Ishenko, L.A. Avakyan, Yan V. Zubavichus, J. Ihlemann, J. Meinertz, E. Pippel, M. Dubiel, L.A. Bugaev, Formation of silver nanoparticles in silicate glass using excimer laser radiation: structural characterization by HRTEM, XRD, EXAFS and optical absorption spectra, J. Alloys Compd. 681 (2016) 307–315, https://doi.org/10.1016/j.jallcom.2016.04.214.
[27] M. Heinz, V.V. Srabionyan, L.A. Avakyan, A.L. Bugaev, A.V. Skidanenko, V.V. Pryadchenko, J. Ihlemann, J. Meinertz, C. Patzig, M. Dubiel, L.A. Bugaev, Formation and implantation of gold nanoparticles by ArF-excimer laser irradiation of gold-coated float glass, J. Alloys Compd. 736 (2018) 152–162, https://doi.org/10.1016/j.jallcom.2017.11.122.
[28] M. Dubiel, M. Heinz, V.V. Srabionyan, V.V. Pryadchenko, L.A. Avakyan, Y.V. Zubavichus, J. Meinertz, J. Ihlemann, L.A. Bugaev, Silver nanoparticles in silicate glass prepared by UV laser irradiation: dependences of size and atomic structure of particles upon irradiation parameters, J. Phys. Conf. Ser. 712 (2016) 12110, https://doi.org/10.1088/1742-6596/712/1/012110.
[29] V.V. Srabionyan, A.L. Bugaev, V.V. Pryadchenko, A.V. Makhiboroda, E.B. Rusakova, L.A. Avakyan, R. Schneider, M. Dubiel, L.A. Bugaev, EXAFS study of changes in atomic structure of silver nanoparticles in soda-lime glass caused by annealing, J. Non-Cryst. Solids 382 (2013) 24–31, https://doi.org/10.1016/j.jnoncrysol.2013.09.025.
[30] G. Smolentsev, A. Soldatov, Quantitative local structure refinement from XANES: multi-dimensional interpolation approach, J. Synchrotron Radiat. 13 (2006) 19–29, https://doi.org/10.1107/S0909049505038975.
[31] G. Smolentsev, A.V. Soldatov, FitIt: new software to extract structural information on the basis of XANES fitting, Comput. Mater. Sci. 39 (2007) 569–574, https://doi.org/10.1016/j.commatsci.2006.08.007.
[32] J.J. Rehr, A.L. Ankudinov, Progress in the theory and interpretation of XANES, Coord. Chem. Rev. 249 (2005) 131–140, https://doi.org/10.1016/j.ccr.2004.02.014.
[33] S.I. Zabinsky, J.J. Rehr, A. Ankudinov, R.C. Albers, M.J. Eller, Multiple-scattering calculations of x-ray-absorption spectra, Phys. Rev. B 52 (1995) 2995–3009, https://doi.org/10.1103/PhysRevB.52.2995.
[34] A.L. Bugaev, A.A. Guda, A. Lazzarini, K.A. Lomachenko, E. Groppo, R. Pellegrini, et al., In situ formation of hydrides and carbides in palladium catalyst: when XANES is better than EXAFS and XRD, Catal. Today 283 (2017) 119–126, https://doi.org/10.1016/j.cattod.2016.02.065.
[35] A.L. Bugaev, A.A. Guda, K.A. Lomachenko, V.V. Srabionyan, L.A. Bugaev, A.V. Soldatov, C. Lamberti, V.P. Dmitriev, J.A. Bokhoven, Temperature- and pressure-dependent hydrogen concentration in supported PdH x nanoparticles by Pd K-Edge x-ray absorption spectroscopy, J. Phys. Chem. C 118 (2014) 10416–10423, https://doi.org/10.1021/jp500734p.
[36] V.V. Srabionyan, A.L. Bugaev, V.V. Pryadchenko, L.A. Avakyan, J.A. van Bokhoven, L.A. Bugaev, EXAFS study of size dependence of atomic structure in palladium nanoparticles, J. Phys. Chem. Solid. 75 (2014) 470–476, https://doi.org/10.1016/j.jpcs.2013.12.012.
[37] L.A. Bugaev, A.P. Sokolenko, H.V. Dmitrienko, A.-M. Flank, Fourier filtration of XANES as a source of quantitative information of interatomic distances and coordination numbers in crystalline minerals and amorphous compounds, Phys. Rev. B 65 (2001) 24105, https://doi.org/10.1103/PhysRevB.65.024105.
[38] V.V. Pryadchenko, V.V. Srabionyan, A.A. Kurzin, N.V. Bulat, D.B. Shemet, L.A. Avakyan, S.V. Belenov, V.A. Volochaev, I. Zizak, V.E. Guterman, L.A. Bugaev, Bimetallic PtCu core-shell nanoparticles in PtCu/C electrocatalysts: structural

and electrochemical characterization, Appl. Catal. A Gen. 525 (2016) 226–236, https://doi.org/10.1016/j.apcata.2016.08.008.
[39] L.A. Avakyan, V.V. Srabionyan, V.V. Pryadchenko, N.V. Bulat, L.A. Bugaev, Construction of three-dimensional models of bimetallic nanoparticles based on X-ray absorption spectroscopy data, Optic Spectrosc. 120 (2016) 926–932, https://doi.org/10.1134/S0030400X16060035.
[40] D.W. Mackowski, M.I. Mishchenko, A multiple sphere T-matrix Fortran code for use on parallel computer clusters, J. Quant. Spectrosc. Radiat. Transf. 112 (2011) 2182–2192, https://doi.org/10.1016/j.jqsrt.2011.02.019.
[41] D. Rioux, S. Vallières, S. Besner, P. Muñoz, E. Mazur, M. Meunier, An analytic model for the dielectric function of Au, Ag, and their alloys, Adv. Opt. Mater. 2 (2014) 176–182, https://doi.org/10.1002/adom.201300457.
[42] S.K. Maurya, Y. Uto, K. Kashihara, N. Yonekura, T. Nakajima, Rapid formation of nanostructures in Au films using a CO 2 laser, Appl. Surf. Sci. 427 (2018) 961–965, https://doi.org/10.1016/j.apsusc.2017.09.044.
[43] N.N. Nedyalkov, R. Nikov, A.O. Dikovska, P.A. Atanasov, G. Obara, M. Obara, Laser annealing of bimetal thin films: a route of fabrication of composite nanostructures, Appl. Surf. Sci. 258 (2012) 9162–9166, https://doi.org/10.1016/j.apsusc.2011.12.023.
[44] Y. Kojima, T. Kato, Nanoparticle formation in Au thin films by electron-beam-induced dewetting, Nanotechnology 19 (2008), 255605, https://doi.org/10.1088/0957-4484/19/25/255605.
[45] C.V. Thompson, Solid-state dewetting of thin films, Annu. Rev. Mater. Res. 42 (2012) 399–434, https://doi.org/10.1146/annurev-matsci-070511-155048.
[46] S.J. Henley, J.D. Carey, S.R.P. Silva, Pulsed-laser-induced nanoscale island formation in thin metal-on-oxide films, Phys. Rev. B 72 (2005), 195408, https://doi.org/10.1103/PhysRevB.72.195408.
[47] D.C. Koningsberger, B.L. Mojet, G.E. van Dorssen, D.E. Ramaker, XAFS spectroscopy; fundamental principles and data analysis, Top. Catal. 10 (2000) 143–155, https://doi.org/10.1023/A:1019105310221.
[48] B. Ravel, M. Newville, ATHENA , ARTEMIS , HEPHAESTUS : data analysis for X-ray absorption spectroscopy using IFEFFIT, J. Synchrotron Radiat. 12 (2005) 537–541, https://doi.org/10.1107/S0909049505012719.
[49] C. Kittel, P. McEuen, Introduction to Solid State Physics, Wiley, New York, 1986.
[50] L.A. Avakyan, M. Heinz, A.V. Skidanenko, K.A. Yablunovski, J. Ihlemann, J. Meinertz, C. Patzig, M. Dubiel, L.A. Bugaev, Insight on agglomerates of gold nanoparticles in glass based on surface plasmon resonance spectrum: study by multi-spheres T-matrix method, J. Phys. Condens. Matter 30 (2018) 45901, https://doi.org/10.1088/1361-648X/aa9fcc.